J Appl Electrochem (2012) 42:901–908
DOI 10.1007/s10800-012-0467-4

ORIGINAL PAPER

Facile synthesis of graphitic carbons decorated with SnO_2 nanoparticles and their application as high capacity lithium-ion battery anodes

A. Ponrouch · M. Sevilla · E. Marchante · M. R. Palacín · A. B. Fuertes

Received: 30 April 2012 / Accepted: 22 July 2012 / Published online: 22 August 2012

Abstract A facile and potentially scalable synthesis route to obtain SnO_2–carbon composites was developed. SnO_2 nanoparticles were deposited on the surface of two types of graphitic carbon: (a) commercial porous graphite (HG) and (b) graphitic carbon nanostructures. The synthesis procedure consists of two simple steps: (i) room temperature formation/deposition of SnO_2 nanocrystals and (ii) thermal treatment at 350 °C to generate SnO_2 nanoparticles (size ~3.5 nm) over the carbon surface. The electrochemical performance of the graphitic carbons and the SnO_2–carbon composites as anode materials in Li-ion rechargeable batteries was investigated. In all cases, tape casting electrode fabrication allowed almost full active material utilization. Good cyclabilities were achieved, with HG and HG–SnO_2 showing capacities of 356 and 545 mAh g^{-1}, respectively after 50 cycles.

Keywords Lithium-ion battery · Graphitic carbon · SnO_2 · Composite

1 Introduction

Although lithium-ion batteries are already well established in the market and used in a wide range of applications, the quest for higher energy density has led scientists to search for alternatives to the standard electrode materials [1]. For the negative electrode, materials that react via conversion reactions (M_aX_b, M being a transition metal and X = O, S, P, N, …) [2] and materials that electrochemically form alloys with Li (Si, Sn, Sb, Al …), [3, 4], have been identified as possible alternatives to carbonaceous negative electrodes. However, alloy-based materials generally suffer from low capacity retention due to the substantial changes in volume that accompany the alloying/de-alloying process. This problem has been addressed by adopting a number of strategies [5], including: (i) downsizing the particles to the nanoscale [6], (ii) use of binary compounds containing elements that do not react with Li and act as non reactive matrix [7], (iii) use of carbon coating to improve electrical conductivity and to induce a strain force on the active material [8, 9] and (iv) formulation of the electrode modifying the nature of the binder, the carbon additives, etc. [10–14]. Among these strategies, the use of nanocomposites containing tin-based compounds (i. e., Sn, SnO_2, and Sn alloys) embedded in a carbonaceous matrix that acts as buffer against any expansion in volume has been the most effective. Indeed, even though the capacity values observed for such electrodes are well below those that might be expected for pure tin, they are significantly higher than those exhibited by standard carbonaceous electrodes. Thus, several studies have been undertaken to develop fabrication procedures for composites containing carbon and tin compounds, fundamentally Sn and SnO_2. To date, most of the reports have focussed on the influence on electrode performance exerted by: (i) the type of carbon used as support (e. g., carbon microbeads, nanotubes, graphene, graphite, etc.) [15–18], (ii) the procedure employed to synthesize the tin oxide nanoparticles (hydrothermal, microwave, etc.) [18, 19], (iii) the amount of tin oxide deposited onto the carbon surface

A. Ponrouch · E. Marchante · M. R. Palacín (✉)
Institut de Ciència de Materials de Barcelona (ICMAB-CSIC), Campus de la UAB, 08193 Bellaterra, Catalonia, Spain
e-mail: rosa.palacin@icmab.es

A. Ponrouch · E. Marchante · M. R. Palacín
ALISTORE_ERI European Research Institute, www.alistore.eu

M. Sevilla · A. B. Fuertes (✉)
Instituto Nacional del Carbón (CSIC), P.O. Box 73, 33080 Oviedo, Spain
e-mail: abefu@incar.csic.es

[20], and (iv) the effect of alloying tin with other active or inactive elements [21, 22].

The procedures used to synthesize SnO_2–carbon composites for their application in lithium-ion batteries are generally complex [19, 23–25]. Moreover, most effective composites use sophisticated non-commercial materials as carbon supports, such as carbon capsules [26], templated mesoporous carbons [27], carbon nanotubes [28] or graphene [29]. These circumstances severely limit the scalability and mass production of SnO_2–carbon composites. Hence, the development of simple and potentially scalable synthesis strategies to fabricate SnO_2–carbon composites represents an important challenge. In this article, an easy and potentially scalable procedure for synthesizing SnO_2–carbon composites by means of an inexpensive and rapid method for incorporating uniform SnO_2 nanoparticles (size <4 nm) onto the surface of highly crystallized carbons is reported. Two types of carbon support were used: (a) a commercially available porous graphite and (b) highly graphitized nanocarbons fabricated by means of a simple procedure as reported elsewhere [30]. The SnO_2–carbon composites thus obtained were tested in lithium batteries. The effect of the electrode formulation procedure was also ascertained by comparing powder electrode technology (a simple mixture consisting of a carbon additive and a tin-based powder material) with tape casted composite electrodes (fabricated with the aid of a binder).

2 Experimental

2.1 Materials preparation

Two types of graphitic carbons were used in these experiments: (i) a commercial porous graphite TIMREX HSAG-300 (Timcal), here denoted as HG, and (ii) graphitic carbon nanostructures prepared in our laboratory and denoted as GCN. The preparation of the GCN material has been reported in detail elsewhere [30]. In brief, it consists of the following steps: (a) the pyrolysis of Fe(II) gluconate dihydrate (Aldrich) under nitrogen up to 900 °C for 3 h, (b) treating the carbon-iron composite under reflux for 2 h in an acid solution of potassium permanganate with a composition (mol ratios) of H_2O:H_2SO_4:$KMnO_4$ = 1:0.02:0.006, c) separation of the solid product by centrifugation and its treatment with HCl (10 %) to remove the MnO_2 formed. After being collected by centrifugation, the solid was washed with abundant distilled water and ethanol. This product is composed almost exclusively of graphitic carbon nanostructures (GCN).

The incorporation of SnO_2 nanoparticles into the graphitic carbon samples was carried out using the procedure reported by Cao et al. [31]. In a typical synthesis, 100 mg of graphitic carbon was dispersed in a solution containing 175 mL of water, 3 mL of HCl (37 %), and 3.5 g $SnCl_2$ (Aldrich). The dispersion was sonicated for 45 min and then stirred for 3.5 h at room temperature. The solid sample was collected by centrifugation, washed with abundant distilled water and dried at 120 °C. Finally, the SnO_2–carbon composites were thermally treated under nitrogen up to 350 °C (5 °C min^{-1}) for 4 h. The final products were denoted as HG–SnO_2 or GCN–SnO_2 depending on the type of graphitic carbon used.

2.2 Characterization of materials

X-ray diffraction (XRD) patterns of the graphitic carbons and graphite–SnO_2 decorated composite were obtained on a Siemens D5000 instrument operating at 40 kV and 20 mA, using CuKa radiation. Adsorption measurements of the samples were performed using a Micromeritics ASAP 2020 volumetric adsorption system. The external surface area (S_{ext}) was estimated by means of the α_s-plot method and a non-graphitized carbon black was used as Ref. [32]. The loadings of SnO_2 into the graphite–SnO_2 decorated composite were determined by thermogravimetric analysis (TGA), which was performed in a C. I. Electronics system under air (heating rate: 10 °C min^{-1}). The morphology of the carbons and composites was examined by scanning (SEM, Zeiss DSM 942) and transmission (TEM, JEOL-2000 FXII) electron microscopy.

2.3 Electrochemical measurements

Two different procedures were used for the fabrication of the composite electrode: (i) 85 % of the active material (referred to hereafter as AM), i. e., GCN, HG, GCN–SnO_2 or HG–SnO_2, was gently mixed with 15 % of Super P carbon (referred to hereafter as Csp from Timcal) by magnetic stirring in cyclohexane overnight, followed by solvent evaporation (denoted powdered electrodes), and (ii) a slurry prepared by mixing 80 wt% of AM, 10 wt% of PVDF as a binder and 10 wt% of Csp in *N*-Methylpyrrolidone (NMP, Aldrich) were tape casted on a 20 μm thick copper foil (Goodfellow) with a 250 μm Doctor-Blade and then subjected to further drying at 120 °C under vacuum (denoted tape casted electrodes).

Swagelok-type cells were then assembled with the working electrode being composed either of (i) 5 mg of the composite powder or (ii) 0.8 cm^2 disk electrodes cut from the tape (typical loading ranging between 1 and 2 mg cm^{-2}) and pressed at 6 tons. A disk of Li metal foil (Chemetal) was used as counter and reference electrode. Two sheets of Whattman GF/d borosilicate fiber glass were used as separator, which was soaked with the electrolyte (ca. 0.5 cm^3 of 1 M $LiPF_6$ in EC:DMC 1:1 (LP30,

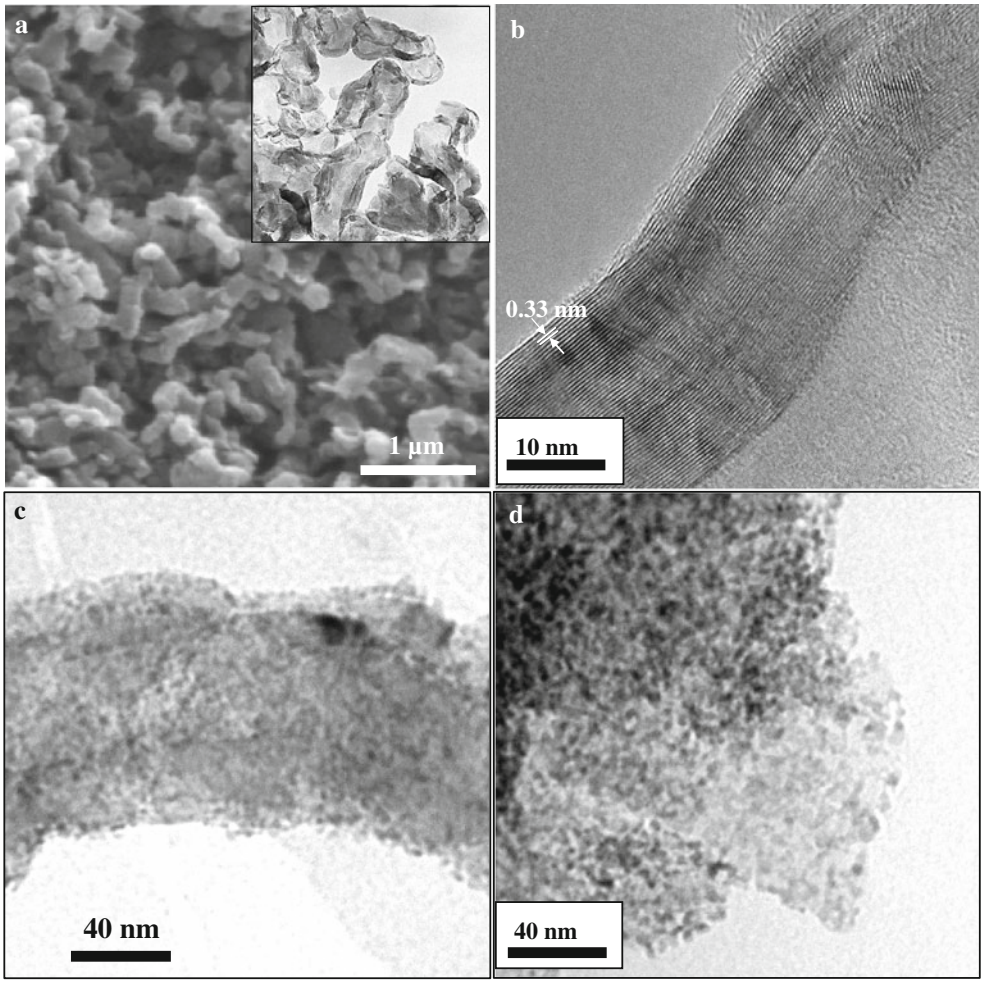

Fig. 1 **a** SEM, (a, *inset*) TEM and **b** HRTEM images of graphitic carbon nanostructures. TEM images of **c** GCN–SnO_2 and **d** HG–SnO_2 composites

Merck)). Electrochemical cycling experiments were carried out in galvanostatic mode with potential limitation (GCPL) between 0.01 and 2 V versus Li^+/Li, at a rate of C/10 (i.e. 1 Li^+ in 10 h), using either an Arbin BT2042 or a MacPile II potentiostat. All the capacities presented here were determined upon reduction and were calculated with respect to the total electrode mass, i.e., per gram of C for HG and GCN and per gram of carbon + SnO_2 for HG–SnO_2 and GCN–SnO_2.

3 Results and discussion

3.1 Physical properties of the graphitic carbons and graphite–SnO_2 decorated composites

The microstructure of the graphitic carbons and the graphite–SnO_2 decorated composites was investigated by SEM, TEM, X-ray diffraction analysis and gas adsorption measurements. The GCN synthesis method has been described in a previous work [30]. The SEM image in Fig. 1a shows that the GCN sample is composed of rod-like nanoparticles (length up to 1 μm, diameter: ~100–150 nm). TEM examination of these nano-rods reveals a corrugated tubular-like morphology and a shell thickness of around 10–25 nm (see inset in Fig. 1a, b). These walls have a high crystallinity, as illustrated by the high-resolution transmission electronic microscopy image in Fig. 1b, which displays well defined (002) lattice fringes. The X-ray diffraction pattern of GCN confirms that this material is highly graphitic (Fig. 2a), exhibiting well-resolved XRD peaks characteristic of a graphitic structure. The structural parameters of the GCN (i.e., d-spacing (002) and the crystallite sizes along the c-axis, L_c, and a-axis, L_a were estimated. The value obtained for the d-spacing (0.339 nm) is larger than the graphite value (0.3354 nm), suggesting that the stacking of the graphene layers has experienced some distortion (turbostratic structure). The sizes of the graphitic crystallites L_c and L_a are around 10 and 27 nm, respectively. The HG graphite also exhibits

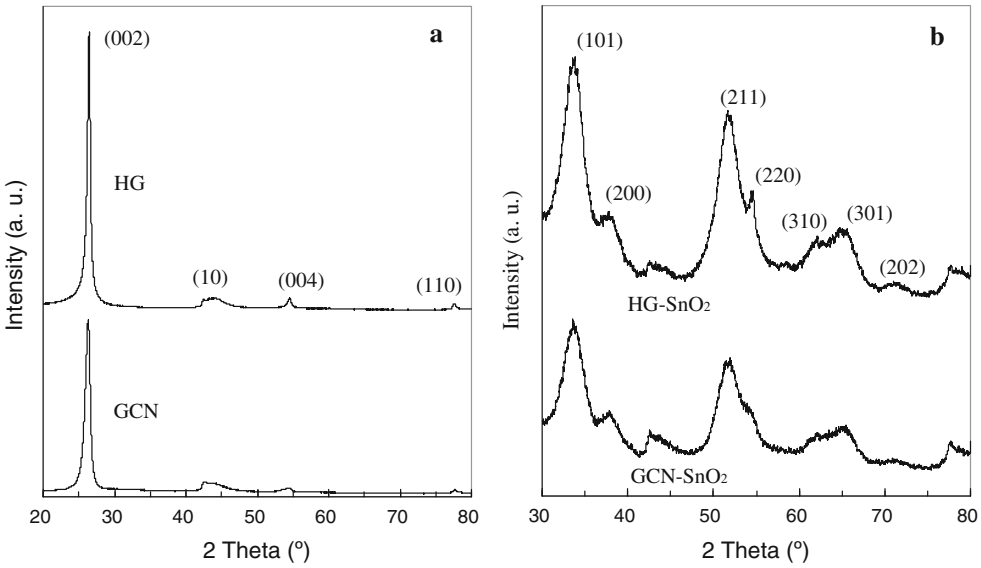

Fig. 2 XRD patterns of: **a** graphitic carbons; **b** carbon–SnO_2 composites

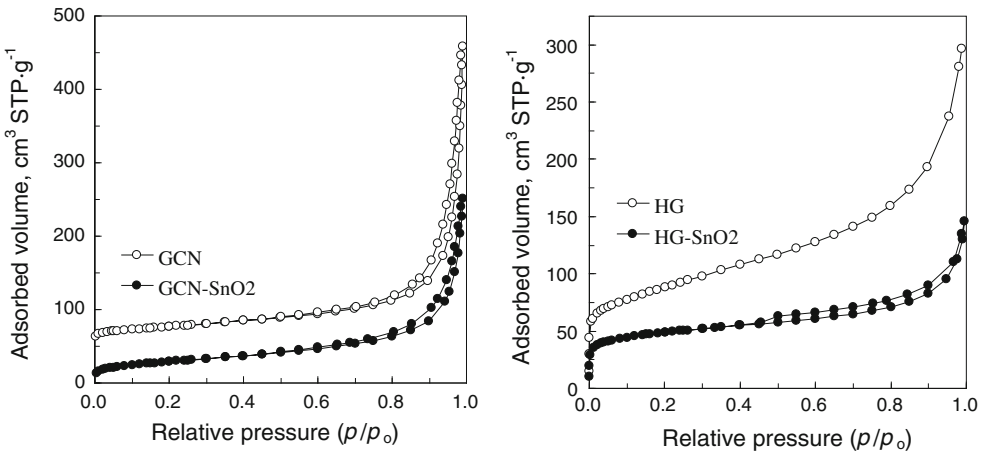

Fig. 3 Nitrogen sorption isotherms of: **a** GCN and GCN–SnO_2; **b** HG and HG–SnO_2 samples. The GCN isotherm has been vertically shifted by 50 $cm^3\ g^{-1}$ for clarity

high crystallinity, as evidenced by the XRD pattern in Fig. 2a, where d(002) = 0.336 nm and the values of the crystallite sizes L_c and L_a are 16 and 41 nm, respectively.

The N_2 sorption isotherm corresponding to GCN exhibits a large nitrogen adsorption uptake at relative pressures >0.99 (see Fig. 3a), which is typical of nanosized materials that do not contain any framework-confined pores. This result is consistent with the morphology of the GCN, as illustrated by SEM and TEM images (Fig. 1a). In the case of the GCN sample, the adsorption only occurs at the outer surface of the nanoparticles so that not surprisingly the BET surface area (96 $m^2\ g^{-1}$) matches the external surface area, as deduced from the α_s-plot analysis (102 $m^2\ g^{-1}$). Given that this material does not contain any internal porosity, it can be inferred that the SnO_2 nanoparticles are deposited exclusively on the outer surface, a characteristic which favors their accessibility to electrolytes and, in consequence, their application in electrochemical devices such as Li-ion batteries. In the case of the HG graphite, however, only ~40 % of the BET surface area (310 $m^2\ g^{-1}$) can be ascribed to the external surface, the rest being associated to the framework-confined pores (>2 nm), as can be seen from the α_s-plot analysis applied to the N_2 sorption isotherm (Fig. 3b).

During the liquid-phase synthesis step, the formation of tin oxide takes place via the oxidation of Sn^{2+} at the surface of the carbon particles and its precipitation as SnO_2 nanocrystals. The overall reaction can be written as:

$$2SnCl_2 + 2H_2O + O_2 \rightarrow 2SnO_2 + 4HCl$$

Thermogravimetric analysis of the synthesized composites reveals that the amount of SnO_2 in the composite is 23 wt% for GCN–SnO_2 and 32 wt% for HG–SnO_2. The subsequent thermal treatment of such as-synthesized composites promotes the growth of the primary SnO_2 nanoclusters into SnO_2 nanoparticles. These nanoparticles are clearly identified by the XRD patterns (Fig. 2b) and TEM images (Fig. 1c, d). Figure 2b shows

the XRD patterns obtained for the GCN–SnO_2 and HG–SnO_2 samples. Both composites exhibit broad peaks, which denote poor crystallinity. These peaks can be assigned to the tetragonal rutile SnO_2 polymorph (JCPDS card no. 41-1445). The crystallite size was estimated through the Scherrer equation considering the FWHM for the (101) peak. The SnO_2 crystallite size thus calculated proved to be similar for both composites, ~3.5 nm. This value is consistent with the diameter of SnO_2 particles inferred by TEM inspection (Fig. 1c, d). Furthermore, these TEM images prove that the SnO_2 nanoparticles are uniformly distributed over the surface of the carbon supports. The nitrogen sorption isotherms obtained for the GCN–SnO_2 and HG–SnO_2 samples are presented in Fig. 3a, b respectively. A reduction in N_2 uptake was observed for both composites in relation to the carbon supports. The BET surface area of the HG–SnO_2 composite was found to be 170 $m^2\ g^{-1}$. This BET surface area on a carbon basis is ~250 $m^2\ g^{-1}$, which indicates a reduction of around 20 % of the surface area of the HG sample and suggests that some of the pores in the HG sample are obstructed by the deposited SnO_2 nanoparticles. In contrast, the BET surface area of the GCN–SnO_2 sample is 106 $m^2\ g^{-1}$ (external surface area: 110 $m^2\ g^{-1}$), while the surface area on a carbon basis is around 140 $m^2\ g^{-1}$. This value is notably higher than the BET surface area of GCN (96 $m^2\ g^{-1}$) and indicates that the deposited SnO_2 nanoparticles have a positive contribution to the surface area of the composite in relation to GCN.

3.2 Electrochemical performance in lithium cells

3.2.1 Graphitic carbons

As mentioned in the previous section, the SnO_2–carbon composites (GCN–SnO_2 and HG–SnO_2) exhibit SnO_2 contents of 23 and 32 wt%, respectively and similar particle sizes (ca. 3.5 nm). The main difference between them is the porosity of the graphitic carbon. Indeed, no internal porosity was observed in the case of GCN, while HG is porous to some extent. The voltage-capacity profiles for powdered electrodes prepared from pure GCN and HG graphitic materials are shown in Fig. 4a. Both exhibit an irreversible sloppy plateau at ca. 0.8 V versus Li^+/Li, corresponding to the formation of a stable SEI during the first cycle [33].

In the case of the pure graphitic carbon electrodes, decomposition of the electrolyte is the main cause of the coulombic inefficiency during the first cycle and is thus proportional to the electrochemically active surface area. The fact that HG and GCN present similar coulombic efficiencies (ca. 25 %) irrespective of whether powder or tape technology used is surprising in view of their very

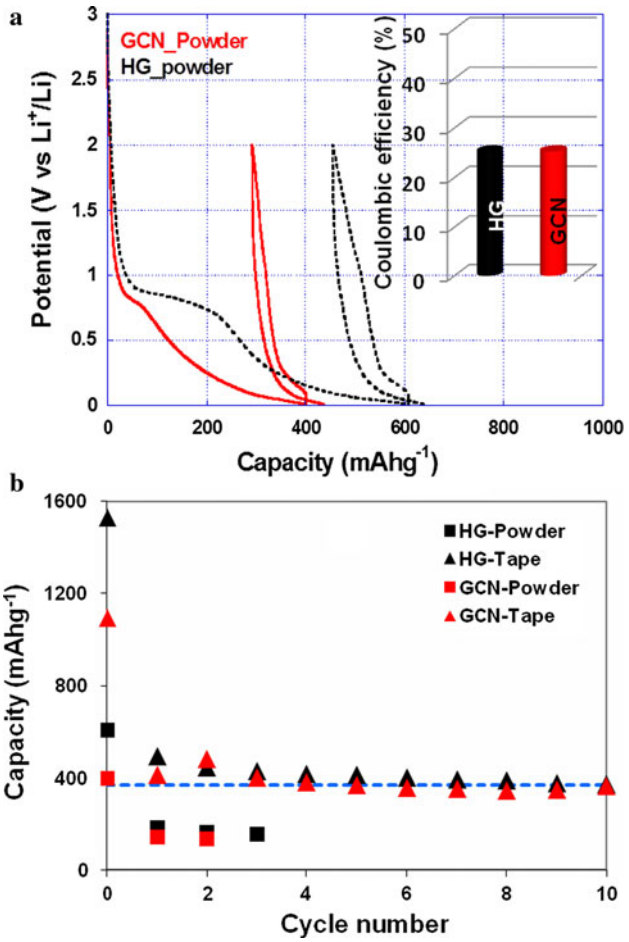

Fig. 4 **a** Voltage versus capacity profiles for GCN and HG (*solid red* and *black dotted curves* respectively), with first cycle coulombic efficiency as inset. **b** Capacity versus cycle number for GCN based electrodes (*red symbols*) and HG based electrodes (*black symbols*). *Square symbols* denote powder electrodes and *triangle symbols* tape casted electrodes. The *blue dotted line* represents the theoretical capacity of graphite (372 mAh g^{-1}). (Color figure online)

different surface areas (ca. 310 and 96 $m^2\ g^{-1}$ for HG and GCN, respectively). However, both can be expected to exhibit the same external surface area, as ~60 % of the surface area of the HG particles is associated with the internal pores. Figure 5 displays a schematic representation of a graphite particle with a uniform pore size. We estimated an approximate SEI volume considering 1 μm carbon particles with 60 % internal porosity and a pore size of 2 nm. Assuming a thickness of 5 nm, the SEI layer [33] volume related to the external surface area is of the order of 1.6×10^{-14} cm^3 and that ascribed to the internal pores one order of magnitude smaller ($\sim 2.3 \times 10^{-15}$ cm^3). Hence, the irreversible capacity in relation to the formation of the SEI layer within the pores is negligible.

The results shown in Fig. 4b (cf. triangle and square symbols) indicate that much higher capacities and lower fading were recorded in the case of the tape casted

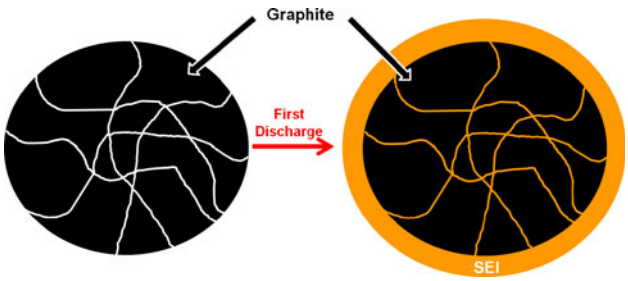

Fig. 5 Schematic representation of the SEI formation in the electrochemically active surface area of a porous carbon particle after the first discharge

electrodes thereby confirming that the formulation of the electrode is of prime importance for achieving the best possible electrochemical performance, even when using materials which do not experience significant volume changes such as graphite [34, 35].

3.2.2 SnO_2–carbon composites

As expected, the incorporation of SnO_2 into the graphitic carbon supports produces a substantial increase in the capacities in all cases (see Fig. 6). This finding further confirms good electrical contact between the SnO_2 nanoparticles and the graphitic material in the as prepared composites. The results shown in Fig. 6b reveal that the potential corresponding to the first discharge sloppy plateau recorded for the SnO_2–carbon composites is higher than that of the graphitic supports. This is presumably due to irreversible reduction in the case of SnO_2 (ca. 1.1 V vs. Li^+/Li), which results in the formation of tin metallic nanoparticles before the formation of Li–Sn alloys [36].

Larger capacity values were obtained with HG–SnO_2 and GCN–SnO_2 powder electrodes, which exhibit first discharge capacities higher than 1,200 mAh g^{-1} (cf. 600 and 400 mAh g^{-1} for HG and GCN respectively). A similar trend was observed for the tape technology: HG and GCN exhibited first discharge capacities of about 1,530 and 1,100 mAh g^{-1} while capacities larger than 1,800 mAh g^{-1} were recorded in the case of the SnO_2–C composites. Coulombic efficiencies were also observed to increase: 25 % in the case of the graphitic carbons and >30 % for the SnO_2–carbon composites (see insets in Figs. 4a, 6a). Slightly higher values were recorded in the case of HG–SnO_2 compared to the GCN–SnO_2 powder electrodes (ca. 43 vs. 33 %, respectively), most probably due to the slightly higher SnO_2 content in HG–SnO_2 compared to GCN–SnO_2. Figure 6b shows the evolution of capacity upon cycling for HG–SnO_2 and GCN–SnO_2. Larger capacities with lower fading during cycling were observed for both samples in the case of electrode preparation via tape technology. Figure 7 displays the plot of capacity

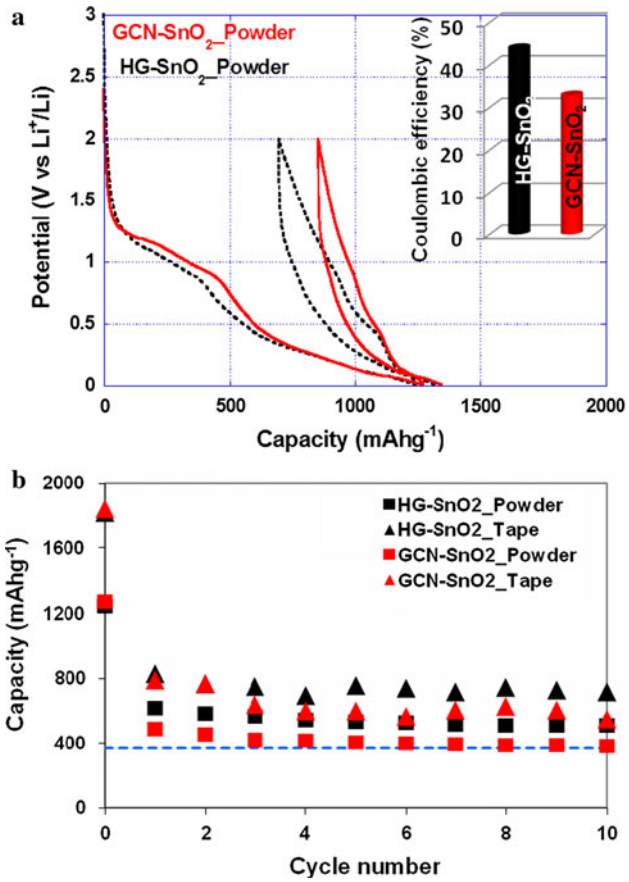

Fig. 6 **a** Voltage versus capacity profiles for GCN–SnO_2 and HG–SnO_2 (*solid red* and *black dotted curves* respectively), with first cycle coulombic efficiency as inset. **b** Capacity versus cycle number for GCN–SnO_2 based electrodes (*red symbols*) and HG–SnO_2 based electrodes (*black symbols*). *Square symbols* denote powder electrodes and *triangle symbols* tape casted electrodes. The *blue dotted line* represents the theoretical capacity of the graphite (372 mAh g^{-1}). (Color figure online)

versus cycle number for the graphitic carbons and the SnO_2–carbon composite tape electrodes over long term cycling. Better capacity retention is observed for HG, with values as high as ca. 356 mAh g^{-1} after 50 cycles (compared to 295 mAh g^{-1} being recorded for GCN, see Fig. 7). This suggests that the porous structure of HG allows easier access to the bulk of the material thereby facilitating the intercalation/deintercalation. Similar differences were observed in the case of the HG–SnO_2 and GCN–SnO_2 composites, their capacities being 545 and 400 mAh g^{-1} respectively after 50 cycles. These values are close to the calculated theoretical capacities for the composite electrodes (570 mAh g^{-1} for HG–SnO_2 and 515 mAh g^{-1} for GCN–SnO_2, which are estimated considering the respective compositions and from the respective theoretical capacities of graphite and SnO_2). As both materials show good capacity retention, the difference between their specific capacities is probably due to the

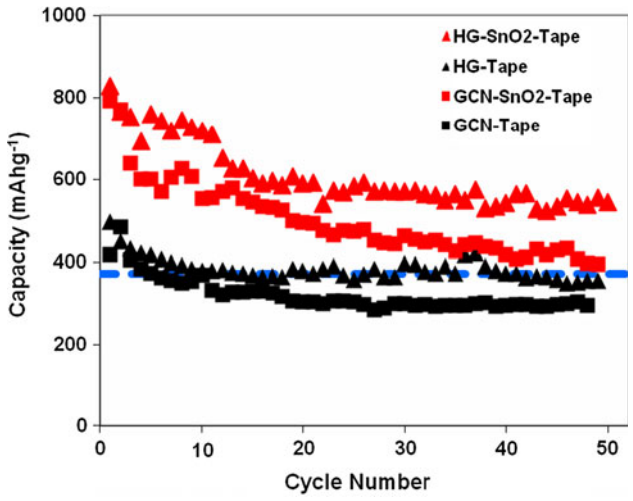

Fig. 7 Capacity versus cycle number for HG (*black triangle*), GCN (*black square scatters*), HG–SnO_2 (*red triangle*) and GCN–SnO_2 (*red square*). In all cases the composite electrodes were tape casted. The *blue dotted line* represents the theoretical capacity of graphite (372 mAh g^{-1}). (Color figure online)

easier access to the bulk of the material in the case of HG and to the slightly higher SnO_2 content in the case of HG–SnO_2 (32 wt%). Overall, these results demonstrate the benefits of tape electrode technology, which allows the achievement of almost the theoretical full capacity for both composites, yielding values that are comparable to the best results found in the literature. Indeed, previously reported specific capacities of around 500 mAh g^{-1} are scarce even though the synthesis protocols usually involved more complex and costly procedures [16, 17, 19, 23–25].

4 Conclusions

A facile, inexpensive and potentially scalable procedure for the synthesis of SnO_2–carbon composites made up of tin oxide nanoparticles that are deposited onto the surface of two types of graphitic carbon is presented. The deposited SnO_2 nanoparticles are highly uniform in size ($\sim$3.5 nm) and they are homogeneously distributed over the surface of the carbon supports. The effectiveness of this synthesis strategy has been demonstrated by applying it to two graphitic carbons with different structural properties, i.e., commercial porous graphite and non-porous graphitic carbon nanocoils prepared in our laboratory. The porosity of the graphite was found to have a significant influence on the irreversible capacity loss on the first cycle, since the formation of the SEI layer is hindered inside the small pores. The tape electrodes containing SnO_2–carbon composites exhibit very good electrochemical performance against lithium. Indeed capacities of 545 mAh g^{-1} for HG–SnO_2 and 400 mAh g^{-1} for GCN–SnO_2 were recorded after 50 cycles. These values are significantly larger than those obtained with bare graphitic supports (356 mAh g^{-1} for HG and 295 mAh g^{-1} for GCN) and compare very well with the results reported in previous published works for composites obtained using complex, time consuming methods where specific capacities of around 500 mAh g^{-1} are scarce.

Acknowledgments We acknowledge the financial support received from the Spanish Ministry of Science and Innovation (MAT2011-24757 and MAT2008-00407). M. S. thanks the Spanish Ministry of Science and Innovation for the award of a Postdoctoral Mobility contract.

References

1. Palacín MR (2009) Recent advances in rechargeable battery materials: a chemist's perspective. Chem Soc Rev 38:2565–2575
2. Cabana J, Monconduit L, Larcher D, Palacín MR (2010) Beyond intercalation-based Li-ion batteries: the state of the art and challenges of electrode materials reacting through conversion reactions. Adv Mater 22:E170–E192
3. Park CM, Kim JM, Kim H, Sohn HJ (2010) Li-alloy based anode materials for Li secondary batteries. Chem Soc Rev 39:3115–3141
4. Zhang WJ (2011) A review of the electrochemical performance of alloy anodes for lithium-ion batteries. J Power Sources 196:13–24
5. Larcher D, Beattie S, Morcrette M, Edström K, Jumas JC, Tarascon JM (2007) Recent findings and prospects in the field of pure metals as negative electrodes for Li-ion batteries. J Mater Chem 17:3759–3772
6. Bruce PG, Scrosati B, Tarascon JM (2008) Nanomaterials for rechargeable lithium batteries. Angew Chem Int Ed 47:2930–2946
7. Beaulieu LY, Dahn JR (2000) The reaction of lithium with Sn-Mn-C intermetallics prepared by mechanical alloying. J Electrochem Soc 147:3237–3241
8. Ryu JH, Kim JW, Sung YE, Oh SM (2004) Failure modes of silicon powder negative electrode in lithium secondary batteries. Electrochem Solid State Lett 7:A306–A309
9. Saint J, Morcrette M, Larcher D, Laffont L, Beattie S, Pérès JP, Talaga D, Couzi M, Tarascon JM (2007) Towards a fundamental understanding of the improved electrochemical performance of silicon-carbon composites. Adv Funct Mater 17:1765–1774
10. Sivasankaran V, Marino C, Chamas M, Soudan P, Guyomard D, Jumas JC, Lippens PE, Monconduit L, Lestriez B (2011) Improvement of intermetallics electrochemical behavior by playing with the composite electrode formulation. J Mater Chem 21:5076–5082
11. Lestriez B (2010) Functions of polymers in composite electrodes of lithium ion batteries.C R Chimie 13:1341–1350
12. Li J, Dahn HM, Krause LJ, Le DB, Dahn JR (2008) Impact of binder choice on the performance of α-Fe_2O_3 as a negative electrode. J Electrochem Soc 155:A812–A816
13. Lestriez B, Desaever S, Danet J, Moreau P, Plée D, Guyomard D (2009) Hierarchical and resilient conductive network of bridged carbon nanotubes and nanofibers for high-energy Si negative electrodes. Electrochem Solid State Lett 12:A76–A80
14. Jiang C, Ichihara M, Honma I, Zhou H (2007) Effect of particle dispersion on high rate performance of nano-sized $Li_4Ti_5O_{12}$ anode. Electrochim Acta 52:6470–6475

15. Wang Y, Su F, Lee JY, Zhao XS (2006) Crystalline carbon hollow spheres, crystalline carbon−SnO_2 Hollow spheres, and crystalline SnO_2 hollow spheres: synthesis and performance in reversible Li-ion storage. Chem Mater 18:1347–1353
16. Fu Y, Ma R, Shu Y, Cao Z, Ma X (2009) Preparation and characterization of SnO_2/carbon nanotube composite for lithium ion battery applications. Mater Lett 63:1946–1948
17. Du Z, Yin X, Zhang M, Hao Q, Wang Y, Wang T (2010) In situ synthesis of SnO_2/graphene nanocomposite and their application as anode material for lithium ion battery. Mater Lett 64:2076–2079
18. Courtel FM, Baranova EA, Abu-Lebdeh Y, Davidson IJ (2010) In situ polyol-assisted synthesis of nano-SnO_2/carbon composite materials as anodes for lithium-ion batteries. J Power Sources 195:2355–2361
19. Lou XW, Chen JS, Chen P, Archer LA (2009) One-pot synthesis of carbon-coated SnO_2 nanocolloids with improved reversible lithium storage properties. Chem Mater 21:2868–2874
20. Li MY, Liu CL, Wang Y, Dong WS (2011) Simple synthesis of carbon/tin oxide composite as anodes for lithium-ion batteries. J Electrochem Soc 158:A296–A301
21. Park CM, Jeon KJ (2011) Porous structured SnSb/C nanocomposites for Li-ion battery anodes.Chem Commun 47:2122–2124
22. Li MY, Liu CL, Shi MR, Dong WS (2011) Nanostructure Sn–Co–C composite lithium ion battery electrode with unique stability and high electrochemical performance. Electrochim Acta 56:3023–3028
23. Chen JS, Cheah YL, Chen YT, Jayaprakash N, Madhavi S, Yang YH, Lou XW (2009) SnO_2 nanoparticles with controlled carbon nanocoating as high-capacity anode materials for lithium-ion batteries. J Phys Chem C 113:20504–20508
24. Chou SL, Wang JZ, Zhong C, Rahman MM, Liu HK, Dou SX (2009) A facile route to carbon-coated SnO_2 nanoparticles combined with a new binder for enhanced cyclability of Li-ion rechargeable batteries. Electrochim Acta 54:7519–7524
25. Liu H, Long D, Liu X, Qiao W, Zhan L, Ling L (2009) Facile synthesis and superior anodic performance of ultrafine SnO_2-containing nanocomposites. Electrochim Acta 54:5782–5788
26. Lou XW, Li CM, Archer LA (2009) Designed synthesis of coaxial SnO_2@carbon hollow nanospheres for highly reversible lithium storage. Adv Mater 21:2536–2539
27. Fan J, Wang T, Yu C, Tu B, Yiang Z, Zhao DY (2004) Ordered, nanostructured tin-based oxides/carbon composite as the negative-electrode material for lithium-ion batteries. Adv Mater 16:1432–1436
28. Wang Y, Zeng HC, Lee JY (2006) Highly reversible lithium storage in porous SnO_2 nanotubes with coaxially grown carbon nanotube overlayers. Adv Mater 18:645–649
29. Paek SM, Yoo EJ, Honma I (2009) Enhanced cyclic performance and lithium storage capacity of SnO_2/graphene nanoporous electrodes with three-dimensionally delaminated flexible structure. Nano Lett 9:72–75
30. Sevilla M, Salinas Martınez-de Lecea C, Valdes-Solís T, Morallon E, Fuertes AB (2008) Solid-phase synthesis of graphitic carbon nanostructures from iron and cobalt gluconates and their utilization as electrocatalyst supports. Phys Chem Chem Phys 10:1433–1442
31. Cao Y, Cao J, Liu J, Zheng M, Shen K (2007) Sonochemical fabrication and photoluminescence properties of ordered mesoporous carbon–tin oxide nanocomposites. Chem Lett 36:254
32. Kruk M, Jaroniec M, Gadkaree KP (1997) Nitrogen adsorption studies of novel synthetic active carbons. J Colloid Interf Sci 192:250–256
33. Aurbach D (2000) Review of selected electrode–solution interactions which determine the performance of Li and Li ion batteries. J Power Sources 89:206–218
34. Courtel FM, Niketic S, Duguay D, Abu-Lebdeh Y, Davidson IJ (2011) Water-soluble binders for MCMB carbon anodes for lithium-ion batteries. J Power Sources 196:2128–2134
35. Ponrouch A, Palacín MR (2011) On the impact of the slurry mixing procedure in the electrochemical performance of composite electrodes for Li-ion batteries: a case study for mesocarbon microbeads (MCMB) graphite and Co_3O_4. J Power Sources 196:9682–9688
36. Courtney IA, Dahn JR (1997) Electrochemical and in situ X-ray diffraction studies of the reaction of lithium with tin oxide composites. J Electrochem Soc 144:2045–2052